PHYSICAL REVIEW D **96,** 103531 (2017)

Analytic approximation for the primordial spectra of single scalar potential models and its use in their reconstruction

D. J. Brooker,[1,*] N. C. Tsamis,[2,†] and R. P. Woodard[1,‡]

[1]*Department of Physics, University of Florida, Gainesville, Florida 32611, USA*
[2]*Institute of Theoretical Physics and Computational Physics, Department of Physics, University of Crete, GR-710 03 Heraklion, Greece*

(Received 9 August 2017; published 20 November 2017)

We give final shape to a recent formalism for deriving the functional forms of the primordial power spectra of single-scalar potential models and theories which are related to them by conformal transformation. An excellent analytic approximation is derived for the nonlocal correction factors which are crucial to capture the "ringing" that can result from features in the potential. We also present the full algorithm for using our representation, including the nonlocal factors, to reconstruct the inflationary geometry from the power spectra.

DOI: 10.1103/PhysRevD.96.103531

I. INTRODUCTION

The simplest models of primordial inflation are based on general relativity (for a spacelike metric $g_{\mu\nu}(x)$) plus a single, minimally coupled scalar $\varphi(x)$,

$$\mathcal{L} = \frac{R\sqrt{-g}}{16\pi G} - \frac{1}{2}\partial_\mu\varphi\partial_\nu\varphi g^{\mu\nu}\sqrt{-g} - V(\varphi)\sqrt{-g}. \quad (1)$$

A key prediction is the generation of tensor [1] and scalar [2] perturbations. These are the first observable quantum gravitational phenomena ever recognized as such [3–5]. They are also our chief means of testing the viability of scalar potential models [6–8], and of reconstructing $V(\varphi)$ [9–11].

Reconstruction is simplest in terms of the Hubble representation [12] using the Hubble parameter $H(t)$ and first slow roll parameter $\epsilon(t)$ of the homogeneous, isotropic and spatially flat background geometry of inflation,[1]

$$ds^2 = -dt^2 + a^2(t)d\vec{x}\cdot d\vec{x} \quad \Rightarrow \quad H(t) \equiv \frac{\dot{a}}{a} > 0,$$
$$\epsilon(t) \equiv -\frac{\dot{H}}{H^2} < 1. \quad (2)$$

Let t_k stand for the time of first horizon crossing, when modes of wave number k obey $k \equiv H(t_k)a(t_k)$. The tensor and scalar power spectra take the form of leading slow roll results at $t = t_k$, multiplied by local slow roll corrections also at $t = t_k$, times nonlocal factors involving times near $t = t_k$ [18,19],

$$\Delta_h^2(k) = \frac{16}{\pi} GH^2(t_k) \times C(\epsilon(t_k)) \times \exp[\tau[\epsilon](k)], \quad (3)$$

$$\Delta_{\mathcal{R}}^2(k) = \frac{GH^2(t_k)}{\pi\epsilon(t_k)} \times C(\epsilon(t_k)) \times \exp[\sigma[\epsilon](k)]. \quad (4)$$

The local slow roll correction $C(\epsilon)$ is,

$$C(\epsilon) \equiv \frac{1}{\pi}\Gamma^2\left(\frac{1}{2} + \frac{1}{1-\epsilon}\right)[2(1-\epsilon)]^{\frac{2}{1-\epsilon}} \approx 1 - \epsilon. \quad (5)$$

The nonlocal correction exponents, $\tau[\epsilon](k)$ and $\sigma[\epsilon](k)$, vanish for $\dot{\epsilon} = 0$ and effectively depend on the geometry only a few e-foldings before and after t_k [18,19].

The purpose of this paper is to rationalize and simplify our formalism for evolving the norms of the mode functions, rather than the mode functions [20], and then to derive an excellent analytic approximation for the nonlocal correction exponents $\tau[\epsilon](k)$ and $\sigma[\epsilon](k)$. We also demonstrate how this approximation can be used to reconstruct the inflationary geometry from the power spectra, even for models which possess features. These topics represent Secs. II–IV, and V, respectively. In Sec. VI we discuss some of the many applications [21,22] this formalism facilitates.

We shall often employ the alternate time parameter provided by $n \equiv \ln[a(t)/a_i]$, the number of e-foldings since inflation's onset. This is superior to the co-moving time t by virtue of being dimensionless and relating evolution to the size of the universe. We shall abuse the notation slightly by writing $H(n)$ and $\epsilon(n)$, instead of the correct but cumbersome expressions $H(t(n))$ and $\epsilon(t(n))$.

---

[*]djbrooker@ufl.edu
[†]tsamis@physics.uoc.gr
[‡]woodard@phys.ufl.edu

[1]The connection to the potential representation is [13–17],

$$\varphi_0(t) = \varphi_0(t_i) \pm \int_{t_i}^{t} dt' H(t')\sqrt{\frac{\epsilon(t')}{4\pi G}} \Leftrightarrow t(\varphi),$$
$$V(\varphi) = \frac{[3-\epsilon(t)]H^2(t)}{8\pi G}\Big|_{t=t(\varphi)}.$$

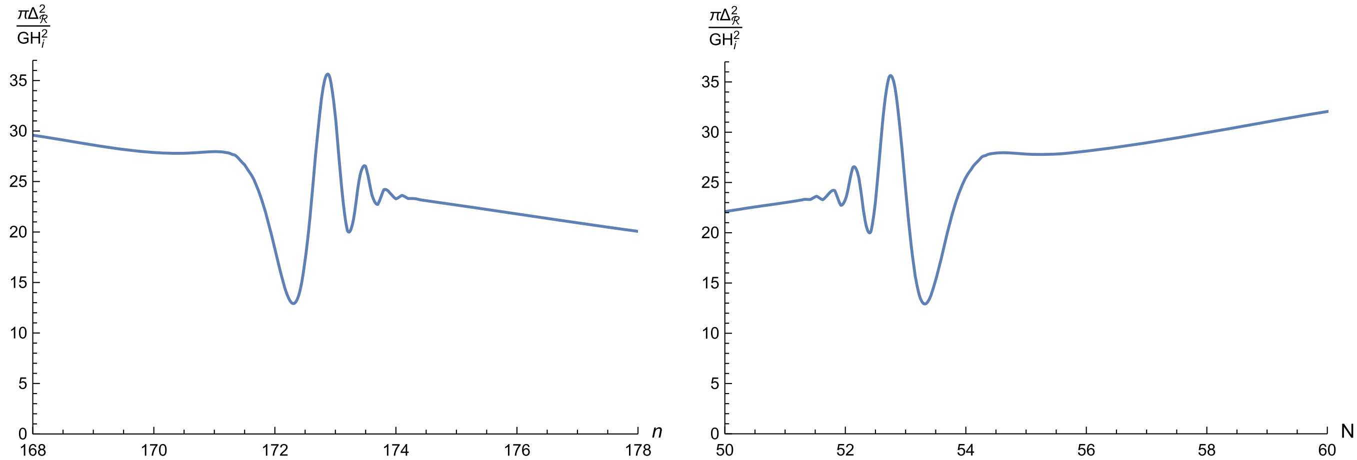

FIG. 1. The left hand graph shows one model's scalar power spectrum as a function of n, the number of e-foldings from the beginning of inflation to first horizon crossing. The right hand graph shows the same power spectrum versus N, the number of e-foldings *until* the end of inflation. Early times correspond to small n and large N, whereas late times correspond to large n and small N. Recall that $n + N = n_e$, where n_e is the total number of e-foldings during inflation.

Which time parameter pertains should be clear from context, and from our exclusive use of ℓ, m, and n to stand for e-foldings. Over-dots represent time derivatives and primes stand for n derivatives,

$$\epsilon = -\frac{\dot{H}}{H^2} = -\frac{H'}{H} \Leftrightarrow H = \frac{H_i}{1 + \int_{t_i}^{t} dt' \epsilon(t')} = H_i \exp\left[-\int_0^n dm \epsilon(m)\right]. \tag{6}$$

We caution readers against confusing n with the common parameter $N \equiv n_e - n$, the number of e-foldings until the end of inflation (at $n = n_e$). Figure 1 illustrates the difference for a model with $n_e \simeq 225$ total e-foldings and features in the range $52 < N < 54$ before the end of inflation.[2]

II. OUR FORMALISM IN GENERAL

The tree order tensor power spectrum is obtained by evolving the graviton mode function $u(t,k)$ past the time of first horizon crossing [9–11],

$$\Delta_h^2(k) = \frac{k^3}{2\pi^2} \times 32\pi G \times 2 \times \lim_{t \gg t_k} |u(t,k)|^2. \tag{7}$$

We do not possess exact solutions for $u(t,k)$ for realistic geometries $\epsilon(t)$, but we do know the evolution equation, the Wronskian and the form at asymptotically early times [9–11,23],

$$\ddot{u} + 3H\dot{u} + \frac{k^2}{a^2} u = 0, \qquad u\dot{u}^* - \dot{u}u^* = \frac{i}{a^3}, \qquad u(t,k) \to \frac{\exp[-ik \int_{t_i}^{t} \frac{dt'}{a(t')}]}{\sqrt{2ka^2(t)}}. \tag{8}$$

Because the power spectrum depends upon the norm-squared, rather than the rapidly-varying phase, it is better to convert (8) into a nonlinear evolution equation for $M(t,k) \equiv |u(t,k)|^2$ [20],

$$\ddot{M} + 3H\dot{M} + \frac{2k^2}{a^2} M = \frac{1}{2M}\left(\dot{M}^2 + \frac{1}{a^6}\right), \qquad M(t,k) \to \frac{1}{2ka^2(t)}. \tag{9}$$

If necessary, the mode function can be easily recovered [19],

$$u(t,k) = \sqrt{M(t,k)} \exp\left[-\frac{i}{2}\int_{t_i}^{t} \frac{dt'}{a^3(t')M(t',k)}\right]. \tag{10}$$

Relation (9) can be improved by changing to the dimensionless time parameter $n = \ln[a(t)/a_i]$,

$$\left(\frac{M'}{M}\right)' + \frac{1}{2}\left(\frac{M'}{M}\right)^2 + (3-\epsilon)\frac{M'}{M} + \frac{2k^2}{H^2a^2} - \frac{1}{2H^2a^6M^2} = 0. \tag{11}$$

A further improvement comes by factoring out an (at this stage) arbitrary approximate solution, $M_0(t,k)$, to derive a damped, driven oscillator equation (with small nonlinearities) for the residual exponent [18],

[2] Because only the last few e-foldings before horizon crossing affect the power spectrum, the features would not have been changed by starting inflation much later so that $n_e \simeq 60$.

$$M = M_0 \times e^{-\frac{1}{2}h} \quad \Rightarrow$$
$$h'' - \frac{\omega'}{\omega} h' + \omega^2 h = S_h + \frac{1}{4} h'^2 - \omega^2 [e^h - 1 - h]. \quad (12)$$

Here the frequency $\omega(n,k)$ and the tensor source $S_h(n,k)$ are,

$$\omega \equiv \frac{1}{Ha^3 M_0} \quad \Rightarrow$$
$$S_h = -2\left(\frac{\omega'}{\omega}\right)' + \left(\frac{\omega'}{\omega}\right)^2 + 2\epsilon' - (3-\epsilon)^2 + \frac{4k^2}{H^2a^2} - \omega^2. \quad (13)$$

It is an amazing fact that an exact Green's function exists for the left-hand side of Eq. (12), valid for *any* choice of the approximate solution M_0 [18],

$$G_h(n;m) = \frac{\theta(n-m)}{\omega(m,k)} \sin\left[\int_0^n d\ell \omega(\ell,k)\right]. \quad (14)$$

This permits us to solve (12) perturbatively $h = h_1 + h_2 + \cdots$ by expanding in the nonlinear terms,

$$h_1(n,k) = \int_0^n dm G_h(n;m) S_h(m,k), \quad (15)$$

$$h_2(n,k) = \int_0^n dm G_h(n;m) \times \left\{\frac{1}{4}[h_1'(m,k)]^2 - \frac{1}{2}[\omega(m,k) h_1(m,k)]^2\right\}. \quad (16)$$

The tree order scalar power spectrum is obtained by evolving the ζ mode function $v(t,k)$ past the time of first horizon crossing [9–11],

$$\Delta^2_{\mathcal{R}}(k) = \frac{k^3}{2\pi^2} \times 4\pi G \times \lim_{t \gg t_k} |v(t,k)|^2. \quad (17)$$

Just as for its tensor cousin, we lack exact solutions for $v(t,k)$ for realistic geometries $\epsilon(t)$, but we do know the evolution equation, the Wronskian and the form at asymptotically early times [9–11,23],

$$\ddot{v} + \left(3H + \frac{\dot{\epsilon}}{\epsilon}\right)\dot{v} + \frac{k^2}{a^2} v = 0, \qquad v\dot{v}^* - \dot{v}v^* = \frac{i}{\epsilon a^3},$$
$$v(t,k) \to \frac{\exp[-ik\int_{t_i}^t \frac{dt'}{a(t')}]}{\sqrt{2k\epsilon(t)a^2(t)}}. \quad (18)$$

Converting to the norm-squared $\mathcal{N}(t,k) \equiv |v(t,k)|^2$ gives [19],

$$\ddot{\mathcal{N}} + \left(3H + \frac{\dot{\epsilon}}{\epsilon}\right)\dot{\mathcal{N}} + \frac{2k^2}{a^2}\mathcal{N} = \frac{1}{2\mathcal{N}}\left(\dot{\mathcal{N}}^2 + \frac{1}{\epsilon^2 a^6}\right),$$
$$\mathcal{N}(t,k) \to \frac{1}{2k\epsilon(t)a^2(t)}. \quad (19)$$

The scalar mode function mode can be recovered from $\mathcal{N}(t,k)$ [19],

$$v(t,k) = \sqrt{\mathcal{N}(t,k)} \exp\left[-\frac{i}{2}\int_{t_i}^t \frac{dt'}{\epsilon(t')a^3(t')\mathcal{N}(t',k)}\right]. \quad (20)$$

Converting from comoving time t to $n = \ln[a(t)/a_i]$ gives,

$$\left(\frac{\mathcal{N}'}{\mathcal{N}}\right)' + \frac{1}{2}\left(\frac{\mathcal{N}'}{\mathcal{N}}\right)^2 + \left(3 - \epsilon + \frac{\epsilon'}{\epsilon}\right)\frac{\mathcal{N}'}{\mathcal{N}} + \frac{2k^2}{H^2a^2} - \frac{1}{2\epsilon^2 H^2 a^6 \mathcal{N}^2} = 0. \quad (21)$$

Factoring out by an arbitrary approximate solution $\mathcal{N}_0(t,k)$ produces another damped, driven oscillator equation for the residual exponent,

$$\mathcal{N} = \mathcal{N}_0 \times e^{-\frac{1}{2}g} \quad \Rightarrow$$
$$g'' - \frac{\Omega'}{\Omega} g' + \Omega^2 g = S_g + \frac{1}{4} g'^2 - \Omega^2 [e^g - 1 - g]. \quad (22)$$

Here the frequency $\Omega(n,k)$ and the scalar source $S_g(n,k)$ are,

$$\Omega \equiv \frac{1}{\epsilon H a^3 \mathcal{N}_0}, \quad (23)$$

$$S_g = -2\left(\frac{\Omega'}{\Omega}\right)' + \left(\frac{\Omega'}{\Omega}\right)^2 + 2\epsilon' - \left(3 - \epsilon + \frac{\epsilon'}{\epsilon}\right)^2 - 2\left(\frac{\epsilon'}{\epsilon}\right)' + \frac{4k^2}{H^2a^2} - \Omega^2. \quad (24)$$

Making the replacement $\omega \to \Omega$ in (14) gives an exact Green's function which is valid for any choice of $\mathcal{N}_0$,

$$G_g(n;m) = \frac{\theta(n-m)}{\Omega(m,k)} \sin\left[\int_0^n d\ell \Omega(\ell,k)\right]. \quad (25)$$

And we can of course develop a perturbative solution to (22) $g = g_1 + g_2 + \cdots$,

$$g_1(n,k) = \int_0^n dm G_g(n;m) S_g(m,k), \quad (26)$$

$$g_2(n,k) = \int_0^n dm G_g(n;m) \times \left\{\frac{1}{4}[g_1'(m,k)]^2 - \frac{1}{2}[\Omega(m,k) g_1(m,k)]^2\right\}. \quad (27)$$

III. CHOOSING $M_0(t,k)$ AND $\mathcal{N}_0(t,k)$ EFFECTIVELY

The formalism of the previous section is valid for all choices of the approximate solutions $M_0(t,k)$ and $\mathcal{N}_0(t,k)$. Of course the correction exponents $h(n,k)$ and $g(n,k)$ will be smaller if the zeroth order solutions are more carefully chosen. In previous work we used the instantaneously constant ϵ solutions [18,19],

$$M_{\rm inst}(t,k) \equiv \frac{z(t,k)\mathcal{H}(\nu(t),z(t,k))}{2ka^2(t)},$$
$$\mathcal{N}_{\rm inst}(t,k) \equiv \frac{z(t,k)\mathcal{H}(\nu(t),z(t,k))}{2k\epsilon(t)a^2(t)}, \tag{28}$$

where we define,

$$\mathcal{H}(\nu,z) \equiv \frac{\pi}{2}|H_\nu^{(1)}(z)|^2, \qquad \nu(t) \equiv \frac{1}{2} + \frac{1}{1-\epsilon(t)},$$
$$z(t,k) \equiv \frac{k}{[1-\epsilon(t)]H(t)a(t)}. \tag{29}$$

However, the choice (28) has the undesirable effect of complicating the late time limits. The physical quantities $M(t,k)$ and $\mathcal{N}(t,k)$ freeze in to constant values soon after first horizon crossing, but continued evolution in $\epsilon(t)$ prevents $M_0(t,k)$ and $\mathcal{N}_0(t,k)$ from approaching constants. Hence the residual exponents $h(n,k)$ and $g(n,k)$ must evolve so as to cancel this effect.

We can make the late time limits simpler by adopting a piecewise choice for the approximate solutions,

$$M_0(t,k) = \theta(t_k - t)M_{\rm inst}(t,k) + \theta(t-t_k)\bar{M}_{\rm inst}(t,k), \tag{30}$$

$$\mathcal{N}_0(t,k) = \theta(t_k - t)\mathcal{N}_{\rm inst}(t,k) + \theta(t-t_k)\bar{\mathcal{N}}_{\rm inst}(t,k). \tag{31}$$

By $\bar{M}_{\rm inst}(t,k)$ and $\bar{N}_{\rm inst}(t,k)$ we mean the solutions which would pertain for the ersatz geometry,

$$\bar{a}(n) = a(n) = a_k e^{\Delta n}, \quad \bar{H}(n) = H_k e^{-\epsilon_k \Delta n}, \quad \bar{\epsilon}(n) = \epsilon_k. \tag{32}$$

Here and henceforth $\Delta n \equiv n - n_k$ stands for the number of e-foldings from horizon crossing. To be explicit about the overlined quantities,

$$\bar{M}_{\rm inst} \equiv \frac{\bar{z}\mathcal{H}(\nu_k,\bar{z})}{2k\bar{a}^2}, \quad \bar{\mathcal{N}}_{\rm inst} \equiv \frac{\bar{z}\mathcal{H}(\nu_k,\bar{z})}{2k\epsilon_k\bar{a}^2}, \quad \bar{z} \equiv \frac{e^{(1-\epsilon_k)\Delta n}}{1-\epsilon_k}. \tag{33}$$

With the choice (30)–(31) the approximate solutions rapidly freeze in to constants,

$$\lim_{t\gg t_k} M_0(t,k) = \frac{H_k^2}{2k^3} \times C(\epsilon_k),$$
$$\lim_{t\gg t_k} \mathcal{N}_0(t,k) = \frac{H_k^2}{2\epsilon_k k^3} \times C(\epsilon_k). \tag{34}$$

This establishes the forms (3)–(4) for the power spectra and fixes the nonlocal correction exponents to,

$$\tau[\epsilon](k) = -\frac{1}{2}\lim_{t\gg t_k} g(t,k), \qquad \sigma[\epsilon](k) = -\frac{1}{2}\lim_{t\gg t_k} h(t,k). \tag{35}$$

It remains to specialize the sources to (30)–(31). First note the simple relation between the scalar and tensor frequencies,

$$\Omega(n,k) = \theta(n_n - n)\omega(n,k) + \theta(n-n_k)\omega(n,k) \times \frac{\epsilon_k}{\epsilon(n)}. \tag{36}$$

This means the scalar source (24) consists of the tensor source (13) minus a handful of terms mostly involving $\epsilon(n)$,

$$\begin{aligned} S_g(n,k) &= S_h(n,k) - 2\theta(n_k - n)\left[\left(\frac{\epsilon'}{\epsilon}\right)' + \frac{1}{2}\left(\frac{\epsilon'}{\epsilon}\right)^2 + (3-\epsilon)\frac{\epsilon'}{\epsilon}\right] \\ &\quad + 2\delta(n-n_k)\frac{\epsilon'}{\epsilon} - 2\theta(n-n_k) \\ &\quad \times \left[\left(3 - \epsilon + \frac{\omega'}{\omega}\right)\frac{\epsilon'}{\epsilon} + \omega^2\left(\frac{\epsilon_k^2}{\epsilon^2} - 1\right)\right]. \end{aligned} \tag{37}$$

To obtain an explicit formula for the tensor source we first note that the tensor frequency is,

$$\omega(n,k) = \theta(n_k - n)\frac{2(1-\epsilon)}{\mathcal{H}(\nu,z)} + \theta(n-n_k)\frac{2(1-\epsilon_k)}{\mathcal{H}(\nu_k,\bar{z})} \times \frac{\bar{H}}{H}. \tag{38}$$

Hence the n derivative of its logarithm is,

$$\frac{\omega'}{\omega} = \theta(n_k - n)\left[-\frac{\epsilon'}{1-\epsilon} - \frac{\mathcal{H}'}{\mathcal{H}}\right] + \theta(n-n_k)\left[\Delta\epsilon - \frac{\bar{\mathcal{H}}'}{\bar{\mathcal{H}}}\right], \tag{39}$$

where $\Delta\epsilon \equiv \epsilon(n) - \epsilon_k$ and $\bar{\mathcal{H}} \equiv \mathcal{H}(\nu_k, \bar{z})$. Before horizon crossing $\nu = \frac{1}{2} + \frac{1}{1-\epsilon}$ is time dependent and $z = k/[(1-\epsilon)Ha]$ so we have,

$$\nu' = \frac{\epsilon'}{(1-\epsilon)^2}, z' = -\Big[1 - \epsilon - \frac{\epsilon'}{1-\epsilon}\Big] z$$
$$\Rightarrow -\frac{\mathcal{H}'}{\mathcal{H}} = -\frac{\epsilon'}{(1-\epsilon)^2}\mathcal{A} + \Big[1 - \epsilon - \frac{\epsilon'}{1-\epsilon}\Big]\mathcal{B}, \qquad (40)$$

where $\mathcal{A}$ and $\mathcal{B}$ involve derivatives of $\mathcal{H}(\nu, z)$ with respect to ν and $\zeta = \ln(z)$,

$$\mathcal{A} \equiv \partial_\nu \ln[\mathcal{H}(\nu, e^\zeta)], \qquad \mathcal{B} \equiv \partial_\zeta \ln[\mathcal{H}(\nu, e^\zeta)]. \qquad (41)$$

The analogous result after horizon crossing is much simpler,

$$-\frac{\bar{\mathcal{H}}'}{\bar{\mathcal{H}}} = (1 - \epsilon_k)\bar{\mathcal{B}}, \qquad (42)$$

where $\bar{\mathcal{B}}$ means $\mathcal{B}$ with ν specialized to ν_k and e^ζ specialized to $\bar{z}$.

Taking the derivative of ω'/ω before horizon crossing,

$$\Big(\frac{\omega'}{\omega}\Big)' = -\frac{\epsilon''}{1-\epsilon} - \frac{\epsilon'^2}{(1-\epsilon)^2} - \Big[\frac{\epsilon''}{(1-\epsilon)^2} + \frac{2\epsilon'^2}{(1-\epsilon)^3}\Big]\mathcal{A} - \Big[\epsilon' + \frac{\epsilon''}{1-\epsilon} + \frac{\epsilon'^2}{(1-\epsilon)^2}\Big]\mathcal{B}$$
$$- \frac{\epsilon'^2}{(1-\epsilon)^4}\mathcal{C} + \frac{2\epsilon'}{(1-\epsilon)^2}\Big[1 - \epsilon - \frac{\epsilon'}{1-\epsilon}\Big]\mathcal{D} - \Big[1 - \epsilon - \frac{\epsilon'}{1-\epsilon}\Big]\mathcal{E}, \qquad (43)$$

requires three second derivatives of $\ln[\mathcal{H}]$,

$$\mathcal{C} \equiv \partial_\nu^2 \ln[\mathcal{H}(\nu, e^\zeta)], \qquad \mathcal{D} \equiv \partial_\zeta \partial_\nu \ln[\mathcal{H}(\nu, e^\zeta)], \qquad \mathcal{E} \equiv \partial_\zeta^2 \ln[\mathcal{H}(\nu, e^\zeta)]. \qquad (44)$$

Bessel's equation and the Wronskian of $H_\nu^{(1)}(e^\zeta)$ imply,

$$2(1-\epsilon)^2\mathcal{E} + (1-\epsilon)^2\mathcal{B}^2 - (3-\epsilon)^2 + 4(1-\epsilon)^2 e^{2\zeta} - \Big(\frac{2(1-\epsilon)}{\mathcal{H}}\Big)^2 = 0. \qquad (45)$$

Substituting relations (39), (40), (43), and (45) in the definition of the tensor source (13) gives,[3]

$$t < t_k \Rightarrow S_{\rm before} = \frac{2\epsilon''}{1-\epsilon}\Big[1 + \frac{\mathcal{A}}{1-\epsilon} + \mathcal{B}\Big] + 2\epsilon'\Big[1 - \frac{\mathcal{A}\mathcal{B}}{1-\epsilon} - \mathcal{B}^2 - \frac{2\mathcal{D}}{1-\epsilon} - 2\mathcal{E}\Big]$$
$$+ \frac{2\epsilon'^2}{(1-\epsilon)^2}\Big\{-\frac{1}{2} + \frac{1}{2}\Big[2 + \frac{\mathcal{A}}{1-\epsilon} + \mathcal{B}\Big]^2 + \frac{\mathcal{A}}{1-\epsilon} + \frac{\mathcal{C}}{(1-\epsilon)^2} + \frac{2\mathcal{D}}{1-\epsilon} + \mathcal{E}\Big\}. \qquad (46)$$

The analogous result after horizon crossing is,

$$t > t_k \Rightarrow S_{\rm after} = 2\Delta\epsilon[3 - \epsilon_k + (1-\epsilon_k)\bar{\mathcal{B}}] + 4\Big[\frac{k^2}{\bar{H}^2 a^2} - \Big(\frac{1-\epsilon_k}{\bar{\mathcal{H}}}\Big)^2\Big]\Big[\frac{\bar{H}^2}{H^2} - 1\Big]. \qquad (47)$$

There is also a jump at horizon crossing so that the complete result is,

$$S_h = \theta(n_k - n)S_{\rm before} - \delta(n - n_k)\frac{2\epsilon'}{1-\epsilon}\Big[1 + \frac{\mathcal{A}}{1-\epsilon} + \mathcal{B}\Big] + \theta(n - n_k)S_{\rm after}. \qquad (48)$$

[3]This result incidentally allows us to write the equations obeyed by the instantaneously constant ϵ solutions (28),

$$\Big(\frac{M'_{\rm inst}}{M_{\rm inst}}\Big)' + \frac{1}{2}\Big(\frac{M'_{\rm inst}}{M_{\rm inst}}\Big)^2 + (3-\epsilon)\frac{M'_{\rm inst}}{M_{\rm inst}} + \frac{2k^2}{H^2a^2} - \frac{1}{2H^2a^6M_{\rm inst}^2} = \frac{1}{2}S_{\rm before},$$
$$\times\Big(\frac{\mathcal{N}'_{\rm inst}}{\mathcal{N}_{\rm inst}}\Big)' + \frac{1}{2}\Big(\frac{\mathcal{N}'_{\rm inst}}{\mathcal{N}_{\rm inst}}\Big)^2 + \Big(3 - \epsilon + \frac{\epsilon'}{\epsilon}\Big)\frac{\mathcal{N}'_{\rm inst}}{\mathcal{N}_{\rm inst}} + \frac{2k^2}{H^2a^2} - \frac{1}{2\epsilon^2H^2a^6\mathcal{N}_{\rm inst}^2}$$
$$= \frac{1}{2}S_{\rm before} - \Big(\frac{\epsilon'}{\epsilon}\Big)' - \frac{1}{2}\Big(\frac{\epsilon'}{\epsilon}\Big)^2 - (3-\epsilon)\frac{\epsilon'}{\epsilon}.$$

Note that the right-hand sides vanish for constant ϵ.

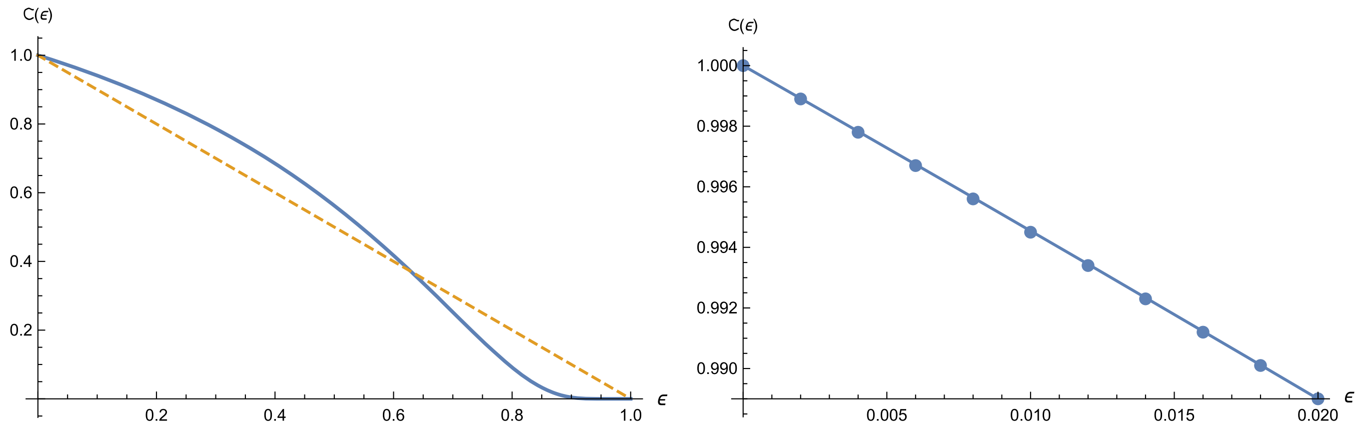

FIG. 2. The left-hand graph shows the local slow roll correction factor $C(\epsilon)$ (solid blue), which was defined in expression (5). Also shown is its global approximation of $1-\epsilon$ (dashed yellow) over the full inflationary range of $0 \leq \epsilon < 1$. The right-hand graph shows $C(\epsilon)$ (solid blue) versus the better approximation of $1-0.55\epsilon$ (large dots) relevant to the range $0 \leq \epsilon < 0.02$ favored by current data.

IV. SIMPLE ANALYTIC APPROXIMATIONS

The exact analytic results of the previous section are valid for all single-scalar models of inflation. However, they can be wonderfully simplified by exploiting the fact that *the first slow roll parameter is very small.* The 95% confidence bound on the tensor-to-scalar ration of $r < 0.12$ [24,25] implies $\epsilon < 0.0075$. This suggests a number of approximations. First, the local slow roll correction factor $C(\epsilon_k)$, defined in (5), may as well be set to unity. From Fig. 2 we see that the bound of $\epsilon < 0.0075$ implies $1.0000 < C(\epsilon_k) < 0.9959$. This is not currently resolvable.

Another excellent approximation is taking $\epsilon = 0$ in the tensor and scalar Green's functions of expressions (14) and (25),

$$\lim_{\epsilon=0} G_h(n;m) = \lim_{\epsilon=0} G_g(n;m) \equiv G_0(n;m) = \frac{\theta(n-m)}{2}[e^{\Delta m} + e^{3\Delta m}] \times \sin[-2\{e^{-\Delta\ell} - \arctan(e^{-\Delta\ell})\}|_m^n], \tag{49}$$

where $\Delta m \equiv m - n_k$ and $\Delta\ell \equiv \ell - n_k$. Note that this expression is valid before and after horizon crossing. An important special case of (49) is when n becomes large, which gives the function $G(e^{\Delta m})$ we define as,

$$G(x) \equiv \frac{1}{2}(x + x^3)\sin\left[\frac{2}{x} - 2\arctan\left(\frac{1}{x}\right)\right]. \tag{50}$$

From the graph in Fig. 3 we see that $G(e^{\Delta n})$ suppresses contributions more than a few e-foldings before horizon crossing.

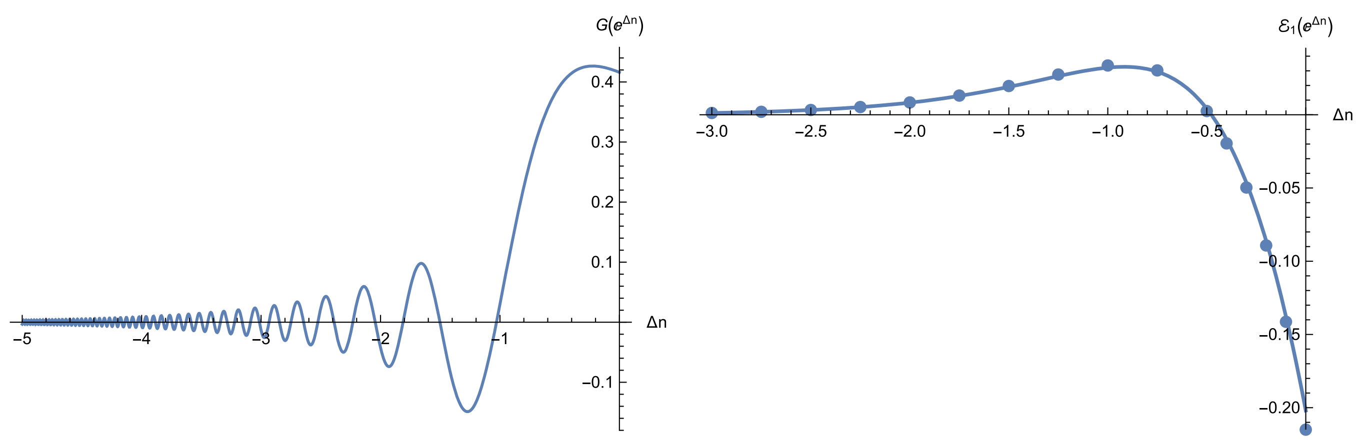

FIG. 3. The left-hand graph shows the $\epsilon = 0$ Green's function $G(e^{\Delta n})$ given in expression (50). The right-hand graph shows the coefficient of $\epsilon''(n)$ in the small ϵ form (58) for $S_h(n,k)$. This function $\mathcal{E}_1(x)$ is defined by expressions (52), (54), and (59). The solid blue curve gives the exact numerical result while the large dots give the approximation resulting from the series expansion on the right-hand side of expression (54).

We can also take $\epsilon = 0$ in $\mathcal{H}$ and the derivatives of it in expressions (41) and (44). This leads to exact results for $\mathcal{H}$, $\mathcal{B}$, and $\mathcal{E}$ in terms of the parameter $x \equiv e^{\Delta n}$,

$$\lim_{\epsilon=0} \mathcal{H} \equiv \mathcal{H}_0(x) = x + x^3, \tag{51}$$

$$\lim_{\epsilon=0} \mathcal{B} \equiv \mathcal{B}_0(x) = \frac{-1 - 3x^2}{1 + x^2}, \tag{52}$$

$$\lim_{\epsilon=0} \mathcal{E} \equiv \mathcal{E}_0(x) = \frac{4x^2}{(1 + x^2)^2}. \tag{53}$$

The three derivatives with respect to ν do not lead to simple expressions even for $\epsilon \to 0$, but they can be well approximated over the range we require by short series expansions in powers of x^2,

$$\lim_{\epsilon=0} \mathcal{A} \equiv \mathcal{A}_0(x) \simeq \frac{1.5x^2 + 1.8x^4 - 1.5x^6 + .63x^8}{1 + x^2}, \tag{54}$$

$$\lim_{\epsilon=0} \mathcal{C} \equiv \mathcal{C}_0(x) \simeq \frac{x^2 + 6.1x^4 - 3.7x^6 + 1.6x^8}{(1 + x^2)^2}, \tag{55}$$

$$\lim_{\epsilon=0} \mathcal{D} \equiv \mathcal{D}_0(x) \simeq \frac{-3x^2 - 6.8x^4 + 5.5x^6 - 2.6x^8}{(1 + x^2)^2}. \tag{56}$$

We can express the ratio of $\bar{H}/H$ in terms of the deviation $\Delta\epsilon(n) \equiv \epsilon(n) - \epsilon_k$,

$$\frac{\bar{H}^2}{H^2} - 1 = \exp\left[2\int_{n_k}^{n} dm \Delta\epsilon(m)\right] - 1 \simeq 2\int_{n_k}^{n} dm \Delta\epsilon(m). \tag{57}$$

All of this gives an approximation for the tensor source (48),

$$\begin{aligned} S_h(n,k) \simeq & -2\theta(-\Delta n)[\epsilon'' \mathcal{E}_1(e^{\Delta n}) + \epsilon'^2 \mathcal{E}_2(e^{\Delta n}) + \epsilon' \mathcal{E}_3(e^{\Delta n})] \\ & + 2\delta(\Delta n)\epsilon' \mathcal{E}_1(1) + 2\theta(\Delta n)\Big\{\Delta\epsilon(n) \\ & + \left(\frac{4 + 2e^{2\Delta n}}{1 + e^{2\Delta n}}\right)\int_{n_k}^{n} dm \Delta\epsilon(m)\Big\}\frac{2}{1 + e^{2\Delta n}}, \end{aligned} \tag{58}$$

where the three coefficient functions are,

$$\mathcal{E}_1(x) = -1 - \mathcal{A}_0(x) - \mathcal{B}_0(x), \tag{59}$$

$$\begin{aligned} \mathcal{E}_2(x) = & \frac{1}{2} - \mathcal{A}_0(x) - \mathcal{C}_0(x) - 2\mathcal{D}_0(x) - \mathcal{E}_0(x) \\ & - \frac{1}{2}[2 + \mathcal{A}_0(x) + \mathcal{B}_0(x)]^2, \end{aligned} \tag{60}$$

$$\mathcal{E}_3(x) = -1 + \mathcal{A}_0(x)\mathcal{B}_0(x) + \mathcal{B}_0^2(x) + 2\mathcal{D}_0(x) + 2\mathcal{E}_0(x). \tag{61}$$

Figures 3 and 4 show the various coefficient functions.

The smallness of ϵ means that the factors of $1/\epsilon$ which occur in the scalar source (37) are hugely important. By comparison we can ignore the $S_h(n,k)$ terms and simply write,

$$\begin{aligned} S_g(n,k) \simeq & -2\theta(-\Delta n)\left[\left(\frac{\epsilon'}{\epsilon}\right)' + \frac{1}{2}\left(\frac{\epsilon'}{\epsilon}\right)^2 + 3\frac{\epsilon'}{\epsilon}\right] \\ & + 2\delta(\Delta n)\frac{\epsilon'}{\epsilon} - 2\theta(\Delta n)\frac{\epsilon'}{\epsilon}\frac{2}{1 + e^{2\Delta n}}. \end{aligned} \tag{62}$$

Because $\epsilon < 0.0075$ we expect S_g to be more than 100 times as strong as S_h.

The approximations (49), (58), and (62) are valid so long as ϵ is small. If we additionally ignore nonlinear terms in the equations for $h(n,k)$ and $g(n,k)$, the correction exponents of expressions (3)–(4) become,

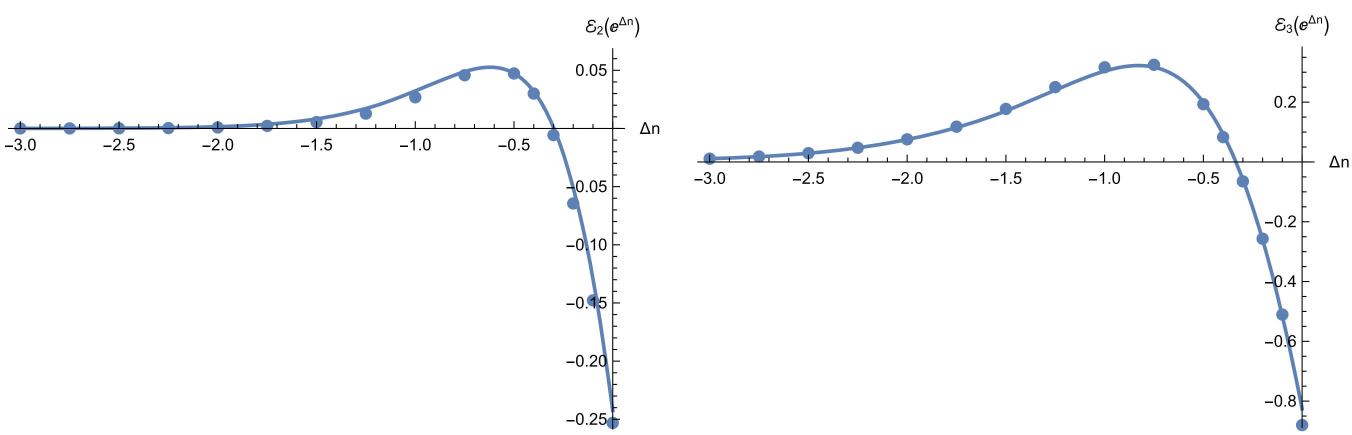

FIG. 4. The coefficients of $[\epsilon'(n)]^2$ (left) and $\epsilon'(n)$ (right) in the small ϵ form (58) for $S_h(n,k)$. In each case the solid blue curve gives the exact numerical result, while the large dots give the result of using the series approximations on the far right of (54)–(56) in expressions (60) and (61).

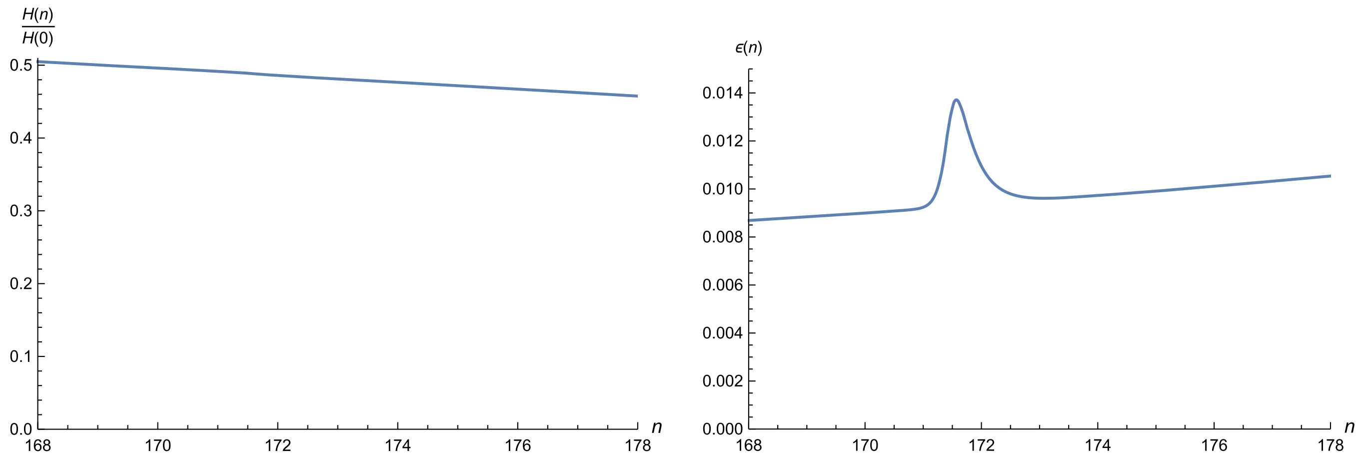

FIG. 5. The left-hand figure shows the Hubble parameter and the right shows the first slow roll parameter for a model with features. This model which was proposed [28,29] to explain the observed features in the scalar power spectrum at $\ell \approx 22$ and $\ell \approx 40$ which are visible in the data reported from both WMAP [27,30,31] and PLANCK [32,33]. Note that the feature has little impact on $H(n)$ but it does lead to a distinct bump in $\epsilon(n)$. Recall that n is the number of e-foldings *from the start* of inflation and that it relates to the number of e-foldings *until the end* of inflation as $N = n_e - n$, where n_e is the total number of inflationary e-foldings.

$$\tau[\epsilon](k) \simeq \int_0^{n_k} dn[\epsilon''(n)\mathcal{E}_1(e^{\Delta n}) + [\epsilon'(n)]^2\mathcal{E}_2(e^{\Delta n}) + \epsilon'(n)\mathcal{E}_3(e^{\Delta n})]G(e^{\Delta n})$$
$$- \epsilon'(n_k)\mathcal{E}_1(1)G(1) - \int_{n_k}^{\infty} dn\left\{\Delta\epsilon(n) + \left(\frac{4+2e^{2\Delta n}}{1+e^{2\Delta n}}\right)\int_{n_k}^{n} dm\Delta\epsilon(m)\right\}\frac{2G(e^{\Delta n})}{1+e^{2\Delta n}}, \tag{63}$$

$$\sigma[\epsilon](k) \simeq \int_0^{n_k} dn\left[\partial_n^2 \ln[\epsilon(n)] + \frac{1}{2}(\partial_n \ln[\epsilon(n)])^2 + 3\partial_n \ln[\epsilon(n)]\right]G(e^{\Delta n})$$
$$- \partial_{n_k}\ln[\epsilon(n_k)]G(1) + \int_{n_k}^{\infty} dn\partial_n \ln[\epsilon(n)]\frac{2G(e^{\Delta n})}{1+e^{2\Delta n}}. \tag{64}$$

Recall that $\Delta n \equiv n - n_k$, $\Delta\epsilon(n) \equiv \epsilon(n) - \epsilon_k$, the Green's function $G(e^{\Delta n})$ was defined in (50), and the coefficient functions $\mathcal{E}_1(e^{\Delta n})$, $\mathcal{E}_2(e^{\Delta n})$ and $\mathcal{E}_3(e^{\Delta n})$ were given in expressions (59)–(61).

How large $\tau[\epsilon](k)$ and $\sigma[\epsilon](k)$ are depends on what the inflationary model predicts for derivatives of $\epsilon(n)$.[4] For example, the slow roll approximation of monomial inflation gives,

$$V(\varphi) = A\varphi^\alpha \Rightarrow \epsilon(n) \simeq \frac{\epsilon_i}{1 - \frac{4}{\alpha}\epsilon_i n}. \tag{65}$$

For these models the various tensor and scalar contributions are small,

$$V(\varphi) = A\varphi^\alpha \quad\Rightarrow\quad \epsilon'' \simeq \frac{32}{\alpha^2}\epsilon^3, \quad \epsilon'^2 \simeq \frac{16}{\alpha^2}\epsilon^4, \quad \epsilon' \simeq \frac{4}{\alpha}\epsilon^2, \tag{66}$$

$$\Rightarrow \quad \left(\frac{\epsilon'}{\epsilon}\right)' \simeq \frac{16}{\alpha^2}\epsilon^2, \qquad \left(\frac{\epsilon'}{\epsilon}\right)^2 \simeq \frac{16}{\alpha^2}\epsilon^2, \qquad \frac{\epsilon'}{\epsilon} \simeq \frac{4}{\alpha}\epsilon. \tag{67}$$

The data disfavors monomial inflation [24–26], but $\tau[\epsilon](k)$ and $\sigma[\epsilon](k)$ will be small for any model which has only slow evolution of $\epsilon(n)$. Much larger effects occur for models with "features," which are transient fluctuations above or below the usual smooth fits [27]. Features imply short-lived changes in $\epsilon(n)$, which do not have much effect on $H(n)$ but can lead to large values of $\epsilon'(n)$ and $\epsilon''(n)$. Figure 5 shows $H(n)$ and $\epsilon(n)$ for a model that was proposed [28,29] to explain a deficit at $\ell \approx 22$, and an excess at $\ell \approx 40$, in the data reported by both WMAP [27,30,31] and PLANCK [32,33]. In the range $171 < n < 172.5$ the scalar experiences a step in its potential which has little effect on $H(n)$ but leads to a noticeable bump in $\epsilon(n)$.

Figure 6 shows the scalar power spectrum for the model of Fig. 5. The left-hand graph compares the exact result to the local slow roll approximation, without including the nonlocal corrections from $\sigma[\epsilon](k)$. Not even the main feature is correct, and the secondary oscillations are completely absent. There is also a small systematic offset

[4] A related issue is the *accuracy* of the approximations (63)–(64). If we ignore nonlinear effects the fractional error in both cases is proportional to ϵ. Because $\epsilon < 0.0075$ the percentage error is less than 1%. If additional accuracy were necessary it would be easy to improve the approximations (63)–(64) by including the next term in the small ϵ expansion.

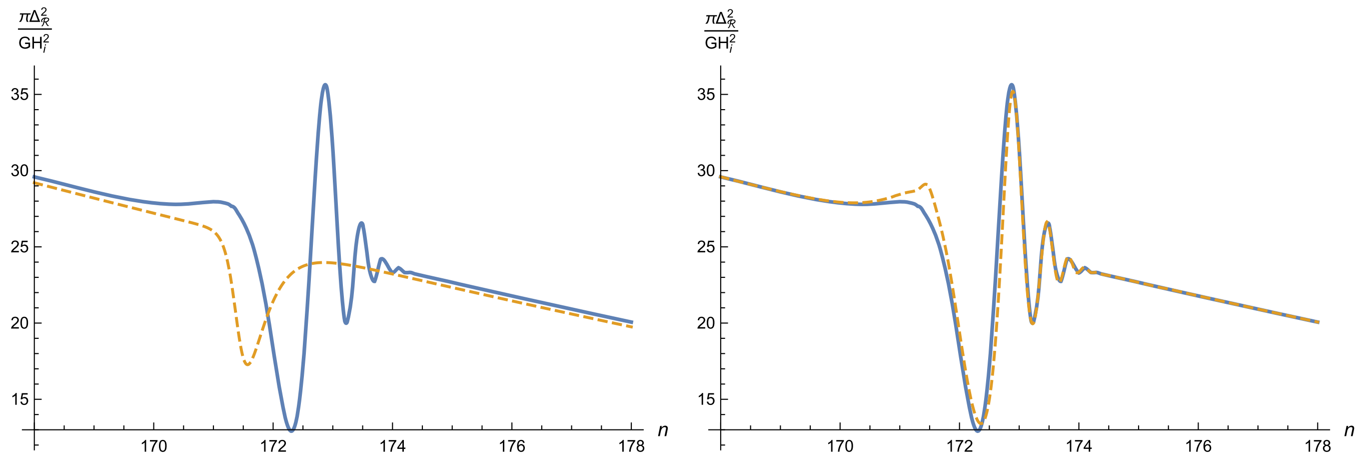

FIG. 6. These graphs show the scalar power spectrum for the model of Fig. 5. The left-hand figure compares the exact result (solid blue) with the local slow roll approximation $\Delta_{\mathcal{R}}^2(k) \approx GH_k^2/\pi\epsilon_k \times C(\epsilon_k)$ (yellow dashed). The right-hand figure compares the exact result (solid blue) with the much better approximation (yellow dashed) obtained from multiplying by $\exp[\sigma[\epsilon](k)]$, using our analytic approximation (64) for $\sigma[\epsilon](k)$. Recall that n is the number of e-foldings *from the start* of inflation and that it relates to the number of e-foldings *until the end* of inflation as $N = n_e - n$, where n_e is the total number of inflationary e-foldings.

before and after the features. The right hand graph shows the effect of adding $\sigma[\epsilon](k)$ with our approximation (64). The agreement is almost perfect, with the small remaining deviations attributable to nonlinear effects. The small offset of the left hand graph (before and after the features) is due to the local slow roll approximation missing the steady growth which $\epsilon(n)$ needs to reach the threshold of $\epsilon = 1$ at which inflation ends. We conclude:

(1) The nonlocal correction $\sigma[\epsilon](k)$ fixes the systematic underprediction of the local slow roll approximation when $\epsilon(n)$ is growing steadily;
(2) The nonlocal correction $\sigma[\epsilon](k)$ makes large and essential contributions when features are present; and
(3) The nonlocal correction $\sigma[\epsilon](k)$ is well approximated by (64).

Figure 7 shows the tensor power spectrum for the model of Fig. 5. The left-hand graph compares the exact result with the local slow roll approximation. The prominent features of the scalar power spectrum which can be seen in Fig. 6 are several hundred times smaller, inverted and phase shifted, but they can just be made out. The right-hand graph compares our approximation (63) for $\tau[\epsilon](k)$ with the exact result. The agreement is again almost perfect, with the small deviations actually attributable to numerical roughness in the interpolation of the exact computation, rather than to any problem with our approximation (63). Correlating tensor features with their much stronger scalar

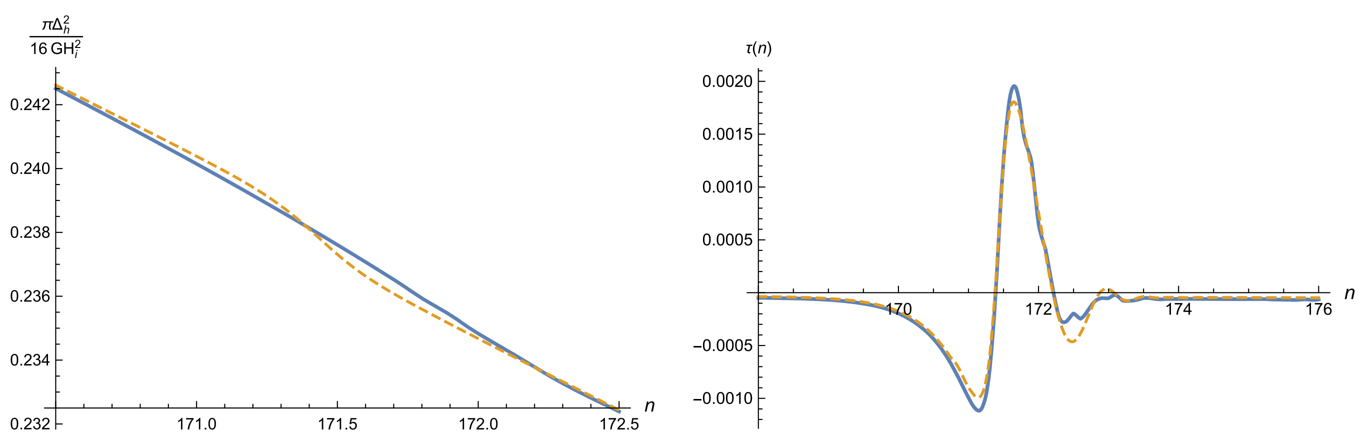

FIG. 7. These graphs show the tensor power spectrum for the model of Figure 5. The left-hand figure compares the exact result (solid blue) with the local slow roll approximation $\Delta_h^2(k) \approx \frac{16}{\pi} GH_k^2 C(\epsilon_k)$ (yellow dashed). The solid blue line on the right-hand graph shows the logarithm of the ratio of $\Delta_h^2(k)$ to its local slow roll approximation. The yellow dashed line gives the nonlocal corrections of expression (63). Recall that n is the number of e-foldings *from the start* of inflation and that it relates to the number of e-foldings *until the end* of inflation as $N = n_e - n$, where n_e is the total number of inflationary e-foldings.

counterparts might be possible in the far future and would represent an impressive confirmation of single-scalar inflation [21].

V. RECONSTRUCTING THE GEOMETRY

We have so far considered the problem of using the inflationary geometry to predict the power spectra. Here we wish to consider the inverse problem of using $\Delta^2_{\mathcal{R}}(k)$ and $\Delta^2_h(k)$ to reconstruct $H(n)$ and $\epsilon(n)$. (The scalar and its potential can be derived from $H(n)$ and $\epsilon(n)$ by the formulae given in footnote 1.) It is well to begin by setting down a few general principles:

(1) Although $\Delta^2_{\mathcal{R}}(k)$ is measured to 3-digit accuracy, the tensor power spectrum has yet to be resolved. When $\Delta^2_h(k)$ is finally detected it will take a number of years before much precision is attained. Therefore, reconstruction should be based on $\Delta^2_{\mathcal{R}}(k)$, with $\Delta^2_h(k)$ used only to fix the integration constant which gives the scale of inflation.

(2) The first slow roll parameter is so small that there is no point in using the exact expression (4) for $\Delta^2_{\mathcal{R}}(k)$. Figure 2 shows that we can ignore the local slow roll correction factor $C(\epsilon_k)$. Although the nonlocal correction exponent $\sigma[\epsilon](k)$ must be included, Fig. 6 shows that the approximation (64) almost perfect.

(3) The fact that $\epsilon(n)$ is small and smooth, with small transients, motivates a hierarchy between H, ϵ and ϵ'/ϵ based on calculus,

$$H(n) = H_i \exp\left[-\int_0^n dm \epsilon(m)\right],$$
$$\epsilon(n) = \epsilon_i \exp\left[\int_0^n dm \frac{\epsilon'(m)}{\epsilon(m)}\right]. \tag{68}$$

Hence $H(n)$ is insensitive to small errors in $\epsilon(n)$, and $\epsilon(n)$ is insensitive to small errors in $\partial_n \ln[\epsilon(n)]$.

We begin by converting from wave number k to n_k, the number of e-foldings since the beginning of inflation that k experienced first horizon crossing. It is also desirable to factor out the scale of inflation $H_i \equiv H(0)$,

$$h(n) \equiv \frac{H(n)}{H_i}, \qquad \delta(n_k) \equiv \frac{\pi \Delta^2_{\mathcal{R}}(k)}{G H_i^2}. \tag{69}$$

(H_i is the single number which would come from the tensor power spectrum.) Based on the three principles we base reconstruction on the formula,

$$\delta(n) \simeq \frac{h^2(n)}{\epsilon(n)} \times \exp\left[\sum_{i=1}^{5} \exp_i(n)\right], \tag{70}$$

where the five exponents follow from our approximation (64) for $\sigma[\epsilon](k)$,

$$\exp_1(n) = -\partial_n \ln[\epsilon(n)] \times G(1), \tag{71}$$

$$\exp_2(n) = \int_0^n dm \partial_m^2 \ln[\epsilon(m)] \times G(e^{m-n}), \tag{72}$$

$$\exp_3(n) = \frac{1}{2}\int_0^n dm [\partial_m \ln[\epsilon(m)]]^2 \times G(e^{m-n}), \tag{73}$$

$$\exp_4(n) = 3\int_0^n dm \partial_m \ln[\epsilon(m)] \times G(e^{m-n}), \tag{74}$$

$$\exp_5(n) = 2\int_n^\infty dm \partial_m \ln[\epsilon(m)] \times \frac{G(e^{m-n})}{1 + e^{2(m-n)}}. \tag{75}$$

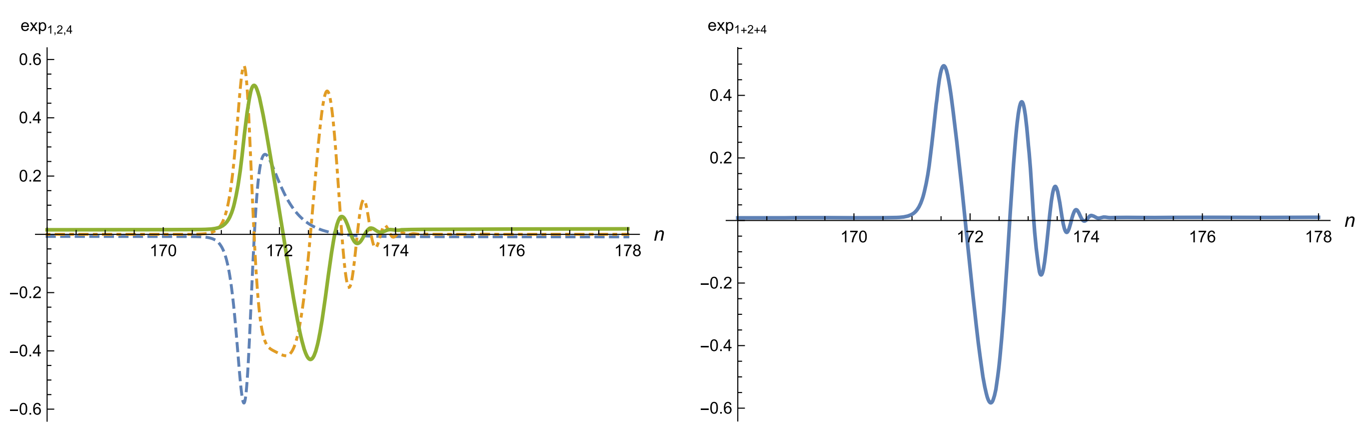

FIG. 8. Numerical values of exponents 1, 2, and 4 for the model of Fig. 5. The left-hand graph gives separate results for expression (71) in dashed blue, expression (72) in dot-dashed yellow, and expression (74) in solid green. The right-hand graph shows the sum of all three exponents. Recall that n is the number of e-foldings *from the start* of inflation and that it relates to the number of e-foldings *until the end* of inflation as $N = n_e - n$, where n_e is the total number of inflationary e-foldings.

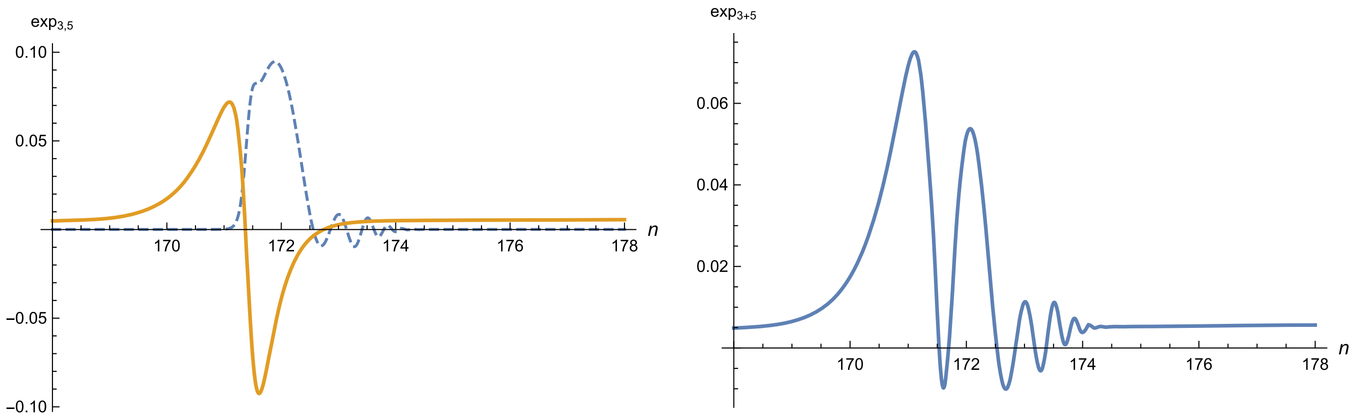

FIG. 9. Numerical values of $\exp_3(n)$ and $\exp_5(n)$ for the model of Fig. 5. The left-hand graph gives separate results for expression (73) in dashed blue, and expression (75) in solid yellow. Note that $\exp_5(n)$ is responsible for correcting the small, systematic underprediction of the slow roll approximation before and after the feature. The right hand graph shows the sum. Recall that n is the number of e-foldings *from the start* of inflation and that it relates to the number of e-foldings *until the end* of inflation as $N = n_e - n$, where n_e is the total number of inflationary e-foldings.

To just reconstruct the Hubble parameter there is no need to include the correction exponents (71)–(75). Using only the leading slow roll terms gives,

$$\delta(n) \simeq \frac{h^2(n)}{\epsilon(n)} \quad \Rightarrow \quad h^2(n) \simeq \frac{1}{1 + \int_0^n \frac{2dm}{\delta(m)}}. \tag{76}$$

Even for the power spectrum of Fig. 6 the reconstruction of $h(n)$ given by expression (76) is barely distinguishable from the left-hand graph of figure 5.

Not all the exponents (71)–(75) are equally important. Figures 8 and 9 show that the set of $\exp_1(n)$, $\exp_2(n)$, and $\exp_4(n)$ are about ten times larger than $\exp_3(n)$ and $\exp_5(n)$ for the model of Fig. 5. That reconstructing features indeed requires the three large exponents is apparent from Fig. 10. Taking the logarithm of (70) and moving the three large exponents to the left gives,

$$\begin{aligned}&[1 + G(1)\partial_n]\ln[\epsilon(n)] \\ &\quad - \int_0^n dm[\partial_m^2 + 3\partial_m]\ln[\epsilon(m)] \times G(e^{m-n}) \\ &\simeq -\ln[\delta(n)] + 2\ln[h(n)] + \exp_3(n) + \exp_5(n).\end{aligned} \tag{77}$$

This becomes a linear, nonlocal equation for $\ln[\epsilon(n)]$ if we drop $\exp_3(n)$ and $\exp_5(n)$ and use expression (76) for the Hubble parameter,

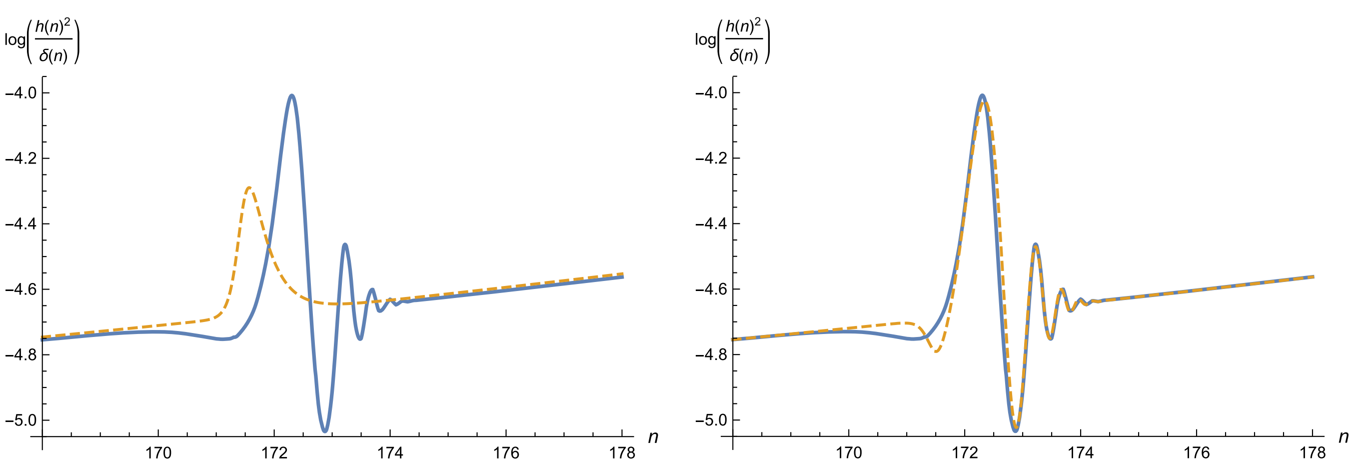

FIG. 10. Various choices for the left-hand side of the first pass reconstruction equation for the model of Fig. 5. The left-hand graph shows the first pass source $-\ln[\delta(n)] + 2\ln[h(n)]$ in solid blue with $\ln[\varepsilon(n)]$ overlaid in dashed yellow. The poor agreement between the two curves is why using just $\ln[\varepsilon(n)]$ as the left hand side of the first pass reconstruction fails to converge when features are present. The right-hand graph shows the much better agreement between the same source (solid blue) and $\ln[\varepsilon(n)] - \exp_1(n) - \exp_2(n) - \exp_4(n)$ (dashed yellow). Recall that n is the number of e-foldings *from the start* of inflation and that it relates to the number of e-foldings *until the end* of inflation as $N = n_e - n$, where n_e is the total number of inflationary e-foldings.

$$\begin{aligned}&[1+G(1)\partial_n]\ln[\epsilon(n)]\\&\quad-\int_0^n dm[\partial_m^2+3\partial_m]\ln[\epsilon(m)]\times G(e^{m-n})\\&\simeq-\ln[\delta(n)]-\ln\left[1+\int_0^n\frac{2dm}{\delta(m)}\right].\end{aligned}\tag{78}$$

The linearity of Eq. (78) means that it can be solved by a Green's function, in spite of being nonlocal. The required Green's function becomes a symmetric function of its arguments if we note from Fig. 3 and expression (50) that $G(e^{n-n_k})$ is essentially zero more than about $N\sim 4$ e-foldings before horizon crossing. The Green's function equation is,

$$\begin{aligned}&[1+G(1)\partial_n]\mathcal{G}(n)\\&\quad-\int_{-N}^n dm(\partial_m^2+3\partial_m)\mathcal{G}(m)\times G(e^{m-n})=\delta(n).\end{aligned}\tag{79}$$

We can solve (78) by integrating against the source on the right-hand side,

$$\ln[\epsilon(n)]=\int_0^\infty dm\mathcal{G}(n-m)\times\mathrm{Source}(m).\tag{80}$$

This might be regarded as the first pass of an iterative solution to (77). After the first pass solution of (78) one would use the resulting $\ln[\epsilon(n)]$ to construct $h(n)$ and to evaluate $\exp_3(n)$ and $\exp_5(n)$ on the right-hand side of (77). Then the same Green's function solution (80) could be used with this more accurate source to find a more accurate $\ln[\epsilon(n)]$, which would lead to a more accurate source, and so on.

We are not able to solve (79) exactly owing to the factor of $G(e^{m-n})$ inside the integral. Consideration of Fig. 3 suggests that this troublesome factor might be approximated as a square wave of width $\Delta=0.8$,

$$G(e^{m-n})\approx G(1)\theta(n-m-\Delta).\tag{81}$$

Making the approximation (81) leads to a still-nonlocal equation,

$$(\partial_n+3)\mathcal{G}_0(n-\Delta)-\alpha\mathcal{G}_0(n)=\frac{\delta(n)}{G(1)},\qquad\alpha\equiv 3-\frac{1}{G(1)}.\tag{82}$$

The "retarded" solution to (82) which avoids exponentially growing terms is,

$$\begin{aligned}\mathcal{G}_0(n)=\frac{e^{3(n+\Delta)}}{G(1)}\sum_{\ell=0}^\infty\frac{1}{\ell!}[\alpha e^{-3\Delta}(n+(\ell+1)\Delta)]^\ell\\\times\theta(n+(\ell+1)\Delta).\end{aligned}\tag{83}$$

Figure 11 shows the result of using just $\mathcal{G}_0(n)$ to reconstruct $\ln[\epsilon(n)]$ with the source taken as the right-hand side of (78).

Further improvement requires a better approximation for the Green's function $\mathcal{G}(n)$. It is instructive to take the Laplace transform, restoring the second argument of the Green's function,

$$\hat{\mathcal{G}}(s;m)\equiv\int_0^\infty dne^{-sn}\mathcal{G}(n-m).\tag{84}$$

The Laplace transform of the Green's function Eq. (79) is,

$$[1+G(1)s-(s+3)s\times\mathcal{I}(s)]\hat{\mathcal{G}}(s;m)=e^{-ms},\tag{85}$$

where we define,

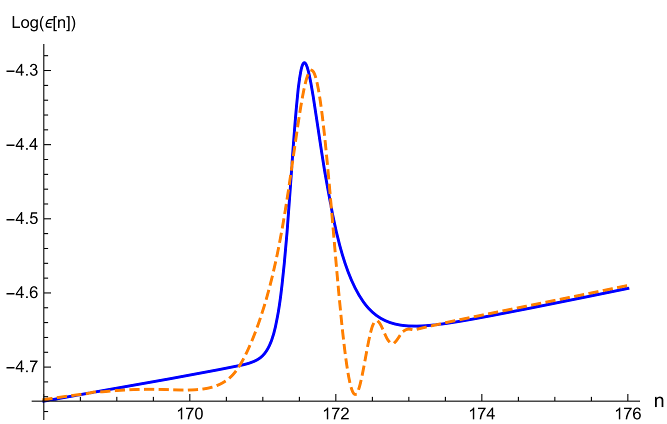

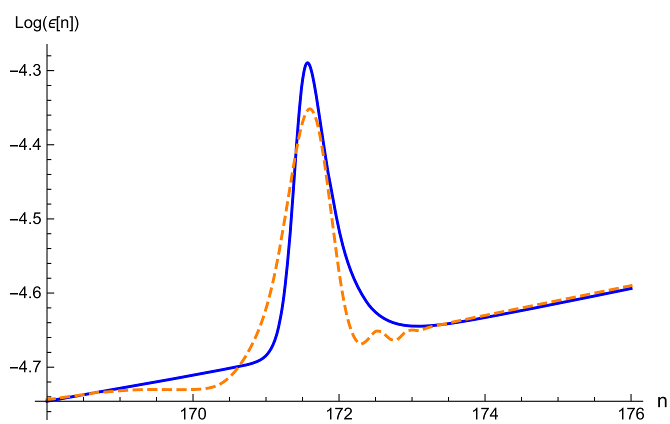

FIG. 11. These graphs show numerical reconstructions of $\ln[\epsilon(n)]$ for the power spectrum of Fig. 6. The solid blue line of the left hand graph shows the exact result while the yellow dashed line gives the result of integrating $\mathcal{G}_0(n-m)$—using the first six terms of the sum over ℓ in expression (83)—against the first pass source on the right-hand side of (78). The right-hand graph shows the result of adding the first order improvement $\mathcal{G}_1(n-m)$—computed using the first four terms of the sum over m in expression (92). Recall that n is the number of e-foldings *from the start* of inflation and that it relates to the number of e-foldings *until the end* of inflation as $N=n_e-n$, where n_e is the total number of inflationary e-foldings.

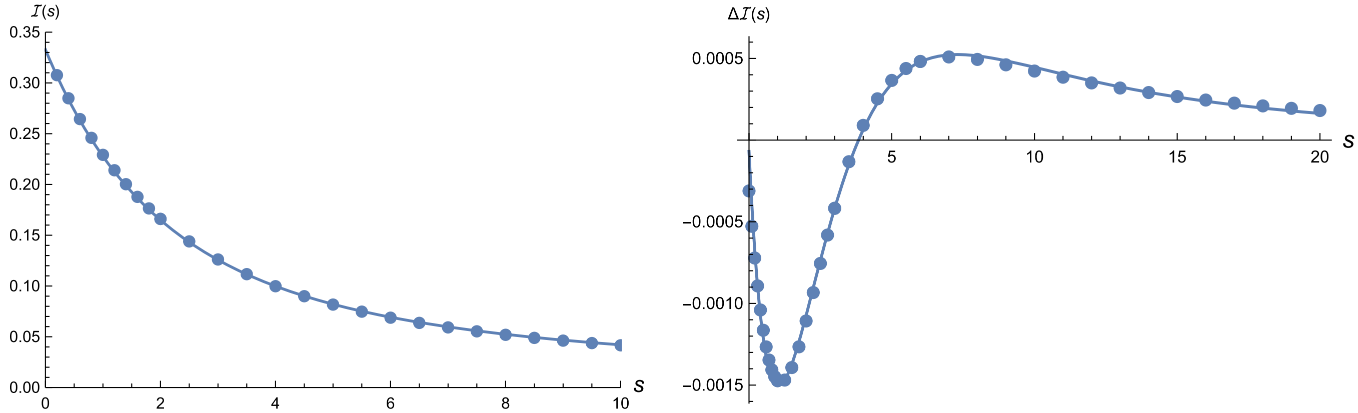

FIG. 12. The solid blue line of the left hand graph shows a numerical evaluation of the integral $\mathcal{I}(s)$ of expression (86). The 0th order approximation $\mathcal{I}_0(s)$ of expression (87) is overlaid in large dots. The solid blue line of the right-hand graph shows the deviation $\Delta\mathcal{I}(s) \equiv \mathcal{I}(s) - \mathcal{I}_0(s)$. Our fit $\mathcal{I}_1(s)$ of expression (88) is overlaid in large dots.

$$\mathcal{I}(s) \equiv \int_0^\infty d\ell e^{-s\ell} \times G(e^{-\ell}). \tag{86}$$

The problem of approximating $\mathcal{G}(n-m)$ is therefore related to the one of approximating (86), and of recognizing the resulting inverse Laplace transform of $\hat{\mathcal{G}}(s;m)$. Making the approximation (81) in (86) gives,

$$\mathcal{I}_0(s) = \frac{G(1)}{s}[1 - e^{-0.8s}]. \tag{87}$$

Figure 12 reveals that this is indeed a good approximation. Figure 12 also shows that the small residual is well fit by the function,

$$\mathcal{I}_1(s) = \frac{0.154}{(s+8.97)^2}\sin[1.76(1 - e^{-0.262(s-3.78)})]. \tag{88}$$

To obtain the first correction to $\mathcal{G}_0(n-m)$ we begin by expanding $\hat{\mathcal{G}}(s;m)$ in powers of $\mathcal{I}_1(s)$,

$$\hat{\mathcal{G}}(s;m) \simeq \frac{e^{-ms}}{G(1)[(s+3)e^{-\Delta s} - \alpha] - s(s+3)\mathcal{I}_1(s)}, \tag{89}$$

$$= \frac{e^{-ms}}{G(1)[(s+3)e^{-\Delta s} - \alpha]} + \frac{s(s+3)\mathcal{I}_1(s)e^{-ms}}{G^2(1)[(s+3)e^{-\Delta s} - \alpha]^2} + \dots, \tag{90}$$

$$\equiv \hat{\mathcal{G}}_0(s;m) + \hat{\mathcal{G}}_1(s;m) + \dots \tag{91}$$

We can recognize the inverse Laplace transform by expanding $\mathcal{I}_1(s)$,

$$\frac{a}{(s+e)^2}\sin[b - be^{-c(s+d)}]$$
$$= \frac{a}{(s+e)^2}\Big\{\sin(b)\sum_{m=0}^\infty \frac{(-1)^m}{(2m)!}[be^{-c(s+d)}]^{2m}$$
$$- \cos(b)\sum_{m=0}^\infty \frac{(-1)^m}{(2m+1)!}[be^{-c(s+d)}]^{2m+1}\Big\}. \tag{92}$$

Figure 11 shows the effect of using $\mathcal{G}_0(n-m)+\mathcal{G}_1(n-m)$ to solve Eq. (78) approximately for $\ln[\epsilon(n)]$.

Figure 11 shows that additional improvements are needed before our technique gives good results for $\partial_n \ln[\epsilon(n)]$ when features are present. However, our results for $\epsilon(n)$ are already reasonable, and those for $h(n)$ are staggeringly accurate. For the model of Fig. 5 the largest percentage error on in reconstructing $\epsilon(n)$ is 2.2%, and the percentage error for $h(n)$ never exceeds 0.04%. This seems considerably better than the general slow roll approximation [34], or techniques based on local expressions [35]. A recent proposal based on inverse-scattering [36] reports percentage errors of $h(n)$ of as much as 2% for flat potentials, and up to 9% when features are present.

It is significant that our Green's function $\mathcal{G}(n-m)$ depends only on the difference of its arguments, and we just need it over a range of about ten e-foldings. Further, its Laplace transform is defined by relations (85)–(86). Figure 12 shows that there is only a single, simple pole on the real axis, somewhat below $s = 3$. If nothing else worked we could therefore evaluate $\mathcal{I}(s_0 + i\omega)$ numerically for some $s_0 > 3$ and then numerically compute the inverse Laplace transform,

$$\mathcal{G}(n-m) = \frac{1}{2\pi i}\int_{-\infty}^\infty d\omega e^{(s_0+i\omega)n}\hat{\mathcal{G}}(s_0+i\omega;m). \tag{93}$$

No matter how time-consuming the computation proved, it would only need to be done once.

VI. EPILOGUE

As the title suggests, this paper gives final expression to our formalism for finding the tree order power spectra by evolving the norm-squared mode functions [20]. Considered purely as a numerical technique this is more efficient than evolving the mode functions because it avoids keeping track of the rapidly fluctuating phase, and because it converges about twice as fast. Nor is anything lost because the phase can be recovered through expressions (10) and (20). Our formalism applies not only to single-scalar inflation but also to any conformally related model, such as $f(R)$ inflation [22], whose power spectra are numerically identical.

Section II reviews our formalism, and explains how to factor out arbitrary approximate solutions (12) and (22). Section III then specializes to what we believe are the best choices (30)–(31) for these approximate solutions. Our results (3)–(4) for the power spectra are exact at this stage, with the nonlocal correction exponents $\tau[\epsilon](k)$ and $\sigma[\epsilon](k)$ given by (35).

Section V makes the approximation that $\epsilon(n)$ is small, and that nonlinear effects can be dropped in the Eqs. (12) and (22) for the residuals. This results in wonderfully simple, analytic approximations (63)–(64) for how the nonlocal correction exponents depend upon $\epsilon(n)$. Figures 6 and 7 exhibit the accuracy of these formulas, even for the model of Fig. 5 which has prominent features. Figure 6 also demonstrates that the local slow roll approximation—$\Delta^2_{\mathcal{R}}(k) \approx \frac{GH_k^2}{\pi\epsilon_k} \times C(\epsilon_k)$—breaks down badly when features are present, and that it systematically underestimates $\Delta^2_{\mathcal{R}}(k)$ even for models without features. The unmistakable conclusions are

(1) That quantitative accuracy requires the nonlocal correction exponents $\tau[\epsilon](k)$ and $\sigma[\epsilon](k)$; and
(2) That our approximations (63)–(64) are valid for any model which is consistent with the bounds on r and on the limits of possible features.

Section V explains how our approximation (64) can be used to reconstruct the geometry from the power spectra. (The scalar and its potential can be recovered from the formulae of footnote 1.) Further improvements are needed for accurate reconstructions for derivatives of the first slow roll parameter, but the undifferentiated parameter is accurate to $\pm 2.2\%$ and our errors for the Hubble parameter never exceed 0.04%. This seems much better than other techniques [34–36].

Our formalism has many applications because it gives explicit, analytic and accurate approximations for how the power spectra depend functionally on the geometry of inflation. For example, our expressions (3)–(4) imply an exact relation for the tensor-to-scalar ratio,

$$r(k) = 16\epsilon_k \exp[-\sigma[\epsilon](k) + \tau[\epsilon](k)], \tag{94}$$

with no local, slow roll corrections. It should be an excellent approximation to drop $\tau[\epsilon](k)$ and employ the analytic approximation (64) for $\sigma[\epsilon](k)$.

We have already mentioned the necessity of including the nonlocal correction exponent $\sigma[\epsilon](k)$ to correctly describe features. Our analytic approximation (64) facilitates precision studies, limited by the accuracy of the data rather than by the cumbersome connection to theory. For example, the model of Fig. 5 was proposed [28,29] to account for the deficit in the scalar power spectrum at $\ell \approx 22$, and the excess at $\ell \approx 40$, which are visible in the data reported from both WMAP [27,30,31] and PLANCK [32,33]. From Fig. 6 we see that the resulting power spectrum indeed has a deficit at $n \approx 172.3$, followed by an excess at $n \approx 172.8$. However, there are weaker features at $n \approx 173.2$ and $n \approx 173.5$. Do the data show any evidence for these weaker features? If not, to what degree does their absence rule out the model of Fig. 5? And what sort of model do the data actually support?

A particularly exciting application of our formalism is to exploit the control it gives over how the mode functions depend upon $\epsilon(n)$ to design a new statistic to cross-correlate features in the power spectrum with non-Gaussianity. This has already been proposed in the context of models with variable speed of sound [37,38], and developed numerically [39], but it can now be done analytically for simple scalar potential models. Of course the idea is that non-Gaussianity measures self-interaction, which is what a step in the potential provides. There may be an observable effect which is not resolvable by generic statistics but could be detected by a precision search.

Another application concerns the far future, after the tensor power spectrum has been well resolved. Our analytic approximations (63)–(64) quantify how the same derivatives of the first slow roll parameter lead to deviations from the local slow roll predictions for the tensor and scalar power spectra. Figure 6 shows that these deviations are strongly present in $\Delta^2_{\mathcal{R}}(k)$ for models with features. The associated tensor features are much weaker, but they can just be made out in Fig. 7. Demonstrating this correlation in the data would represent an impressive check on single-scalar inflation.

In the even farther future it may be possible to resolve one loop corrections [23]. Comparing these with theory obviously requires a precision determination of the tree order effect, which is of course possible once the model of inflation has been fixed. However, one also needs to be able to extract the potentially large factors of $1/\epsilon(n)$ from the ζ propagator, and our formalism is ideal for that.

ACKNOWLEDGMENTS

This work was partially supported by the European Union's Seventh Framework Programme (FP7-REGPOT-2012-2013-1) under grant agreement number 316165; by the European Union's Horizon 2020 Programme under Grant Agreement No. 669288-SM-GRAV-ERC-2014-ADG; by NSF Grant No. PHY-1506513; and by the UF's Institute for Fundamental Theory.

[1] A. A. Starobinsky, Spectrum of relict gravitational radiation and the early state of the universe, Pis'ma Zh. Eksp. Teor. Fiz. **30**, 719 (1979) [JETP Lett. **30**, 682 (1979)].

[2] V. F. Mukhanov and G. V. Chibisov, Quantum fluctuation and nonsingular universe. (In Russian), Pis'ma Zh. Eksp. Teor. Fiz. **33**, 549 (1981) [JETP Lett. **33**, 532 (1981)].

[3] R. P. Woodard, How far are we from the quantum theory of gravity?, Rep. Prog. Phys. **72**, 126002 (2009).

[4] A. Ashoorioon, P. S. Bhupal Dev, and A. Mazumdar, Implications of purely classical gravity for inflationary tensor modes, Mod. Phys. Lett. A **29**, 1450163 (2014).

[5] L. M. Krauss and F. Wilczek, Using cosmology to establish the quantization of gravity, Phys. Rev. D **89**, 047501 (2014).

[6] D. Polarski and A. A. Starobinsky, Structure of primordial gravitational waves spectrum in a double inflationary model, Phys. Lett. B **356**, 196 (1995).

[7] J. Garcia-Bellido and D. Wands, Constraints from inflation on scalar-tensor gravity theories, Phys. Rev. D **52**, 6739 (1995).

[8] M. Sasaki and E. D. Stewart, A general analytic formula for the spectral index of the density perturbations produced during inflation, Prog. Theor. Phys. **95**, 71 (1996).

[9] V. F. Mukhanov, H. A. Feldman, and R. H. Brandenberger, Theory of cosmological perturbations. Part 1. Classical perturbations. Part 2. Quantum theory of perturbations. Part 3. Extensions, Phys. Rep. **215**, 203 (1992).

[10] A. R. Liddle and D. H. Lyth, The cold dark matter density perturbation, Phys. Rep. **231**, 1 (1993).

[11] J. E. Lidsey, A. R. Liddle, E. W. Kolb, E. J. Copeland, T. Barreiro, and M. Abney, Reconstructing the inflation potential: An overview, Rev. Mod. Phys. **69**, 373 (1997).

[12] A. R. Liddle, P. Parsons, and J. D. Barrow, Formalizing the slow roll approximation in inflation, Phys. Rev. D **50**, 7222 (1994).

[13] N. C. Tsamis and R. P. Woodard, Nonperturbative models for the quantum gravitational back reaction on inflation, Ann. Phys. (N.Y.) **267**, 145 (1998).

[14] T. D. Saini, S. Raychaudhury, V. Sahni, and A. A. Starobinsky, Reconstructing the Cosmic Equation of State from Supernova Distances, Phys. Rev. Lett. **85**, 1162 (2000).

[15] S. Nojiri and S. D. Odintsov, Unifying phantom inflation with late-time acceleration: Scalar phantom-non-phantom transition model and generalized holographic dark energy, Gen. Relativ. Gravit. **38**, 1285 (2006).

[16] R. P. Woodard, Avoiding dark energy with 1/r modifications of gravity, Lect. Notes Phys. **720**, 403 (2007).

[17] Z. K. Guo, N. Ohta, and Y. Z. Zhang, Parametrizations of the dark energy density and scalar potentials, Mod. Phys. Lett. A **22**, 883 (2007).

[18] D. J. Brooker, N. C. Tsamis, and R. P. Woodard, Precision predictions for the primordial power spectra of scalar potential models of inflation, Phys. Rev. D **93**, 043503 (2016).

[19] D. J. Brooker, N. C. Tsamis, and R. P. Woodard, Effect of features on the functional form of the scalar power spectrum, Phys. Rev. D **94**, 044020 (2016).

[20] M. G. Romania, N. C. Tsamis, and R. P. Woodard, Computing the primordial power spectra directly, J. Cosmol. Astropart. Phys. 08 (2012) 029.

[21] D. J. Brooker, N. C. Tsamis, and R. P. Woodard, Improving the single scalar consistency relation, Phys. Lett. B **773**, 225 (2017).

[22] D. J. Brooker, S. D. Odintsov, and R. P. Woodard, Precision predictions for the primordial power spectra from $f(R)$ models of inflation, Nucl. Phys. **B911**, 318 (2016).

[23] R. P. Woodard, Perturbative quantum gravity comes of age, Int. J. Mod. Phys. D **23**, 1430020 (2014).

[24] P. A. R. Ade *et al.* (BICEP2 and Planck Collaborations), Joint Analysis of BICEP2/Keck Array and Planck Data, Phys. Rev. Lett. **114**, 101301 (2015).

[25] P. A. R. Ade *et al.* (Planck Collaboration), Planck 2015 results. XIII. Cosmological parameters, Astron. Astrophys. **594**, A13 (2016).

[26] P. A. R. Ade *et al.* (Planck Collaboration), Planck 2015 results. XX. Constraints on inflation, Astron. Astrophys. **594**, A20 (2016).

[27] L. Covi, J. Hamann, A. Melchiorri, A. Slosar, and I. Sorbera, Inflation and WMAP three year data: Features have a future!, Phys. Rev. D **74**, 083509 (2006).

[28] J. A. Adams, B. Cresswell, and R. Easther, Inflationary perturbations from a potential with a step, Phys. Rev. D **64**, 123514 (2001).

[29] M. J. Mortonson, C. Dvorkin, H. V. Peiris, and W. Hu, CMB polarization features from inflation versus reionization, Phys. Rev. D **79**, 103519 (2009).

[30] J. Hamann, L. Covi, A. Melchiorri, and A. Slosar, New constraints on oscillations in the primordial spectrum of inflationary perturbations, Phys. Rev. D **76**, 023503 (2007).

[31] D. K. Hazra, M. Aich, R. K. Jain, L. Sriramkumar, and T. Souradeep, Primordial features due to a step in the inflaton potential, J. Cosmol. Astropart. Phys. 10 (2010) 008.

[32] D. K. Hazra, A. Shafieloo, G. F. Smoot, and A. A. Starobinsky, Wiggly whipped inflation, J. Cosmol. Astropart. Phys. 08 (2014) 048.

[33] D. K. Hazra, A. Shafieloo, G. F. Smoot, and A. A. Starobinsky, Primordial features and Planck polarization, J. Cosmol. Astropart. Phys. 09 (2016) 009.

[34] K. Kadota, S. Dodelson, W. Hu, and E. D. Stewart, Precision of inflaton potential reconstruction from CMB using the general slow-roll approximation, Phys. Rev. D **72**, 023510 (2005).

[35] J. D. Barrow and A. Paliathanasis, Reconstructions of the dark-energy equation of state and the inflationary potential, arXiv:1611.06680.

[36] J. Mastache, F. Zago, and A. Kosowsky, Inflationary dynamics reconstruction via inverse-scattering theory, Phys. Rev. D **95**, 063511 (2017).

[37] A. Achcarro, J. O. Gong, G. A. Palma, and S. P. Patil, Correlating features in the primordial spectra, Phys. Rev. D **87**, 121301 (2013).

[38] J. Torrado, B. Hu, and A. Achucarro, Robust predictions for an oscillatory bispectrum in Planck 2015 data from transient reductions in the speed of sound of the inflaton, Phys. Rev. D **96**, 083515 (2017).

[39] D. K. Hazra, L. Sriramkumar, and J. Martin, BINGO: A code for the efficient computation of the scalar bi-spectrum, J. Cosmol. Astropart. Phys. 05 (2013) 026.